Monthly Notices of the ROYAL ASTRONOMICAL SOCIETY

MNRAS **542,** 203–214 (2025) https://doi.org/10.1093/mnras/staf1203
Advance Access publication 2025 July 12

A new long-period radio transient: discovery of pulses repeating every 1.16 h from ASKAP J175534.9−252749.1

Samuel J. McSweeney [1]★ Natasha Hurley-Walker,[1] Csanád Horváth,[1] Akash Anumarlapudi,[2] Angie Waszewski,[1,3] Dougal Dobie [4,5] David L. Kaplan [2] John Morgan,[3] Kovi Rose [4,6] and Ziteng Wang [1]

[1]*International Centre for Radio Astronomy Research, Curtin University, 1 Turner Avenue, Bentley, WA 6102, Australia*
[2]*Department of Physics, University of Wisconsin-Milwaukee, 3135 North Maryland Avenue, Milwaukee, WI 53201, USA*
[3]*CSIRO Space and Astronomy, 26 Dick Perry Avenue, Kensington, WA 6151, Australia*
[4]*Sydney Institute for Astronomy, School of Physics (A28), Physics Road, Camperdown, NSW 2006, Australia*
[5]*ARC Centre of Excellence for Gravitational Wave Discovery (OzGrav), Level 9 AMDC Building, Swinburne University of Technology, Hawthorn, VIC 3122, Australia*
[6]*Australian Telescope National Facility CSIRO, 26 Pembroke Road, Marsfield, NSW 2122, Australia*

Accepted 2025 July 18. Received 2025 July 13; in original form 2025 June 5

ABSTRACT

We report the discovery of several new pulses from the source ASKAP J175534.9−252749.1 (J1755−2527), originally identified from a single 2-min long pulse, confirming it as a long-period transient (LPT) with a period of ∼1.16 h. The pulses are significantly scattered, consistent with Galactic electron density models. Two of the new pulses also had measurable polarization, but unlike the originally detected pulse, the polarization angle does not behave as expected from the rotating vector model. We interpret historical non-detections of J1755−2527 as an intrinsic intermittency that occurs on month-long time-scales, and discuss possible causes. We conjecture that, like some other LPTs with periods $\gtrsim 1$ h, J1755−2527 may host a white dwarf in a binary orbit, but note that its period is marginally shorter than the canonical orbital period minimum of cataclysmic variables. Our work highlights the importance of additional observations in establishing the nature of unusual radio-emitting objects.

Key words: white dwarfs – radio continuum: transients.

1 INTRODUCTION

ASKAP J175534.9−252749.1 (hereafter, J1755−2527) is a transient radio source (Dobie et al. 2024, hereafter Paper I) discovered in the Variables and Slow Transients (VAST) survey (Murphy et al. 2013). A single highly polarized pulse was observed, lasting approximately 2 min, exhibiting a steep spectrum ($\alpha = -3.1$, for flux density $S_\nu \propto \nu^\alpha$). Extensive follow-up in new and archival data at multiple wavelengths turned up no other pulses. Despite this, the authors concluded that J1755−2527 was most likely a long-period transient (LPT), a newly emerging class of radio source with periods ranging from minutes to hours (see e.g. Hurley-Walker et al. 2022, 2023; Caleb et al. 2024). Without additional evidence, however, J1755−2527 has heretofore not been classified as an LPT in current catalogues.

Although optical observations have provided compelling evidence that at least some LPTs are detached, possibly strongly magnetic, white dwarf/M-dwarf (WD + MD) binary systems (Hurley-Walker et al. 2024; de Ruiter et al. 2025; Rodriguez 2025), it remains unclear if this model can account for all known LPTs (e.g. Rea et al. 2022; Lee et al. 2025). Optical follow-up is challenging for J1755−2527, which is situated very close to the Galactic plane ($b = -0.^\circ12$), at a distance of ∼4.7 kpc (Paper I). Unsurprisingly, archival searches at J1755−2527's location did not turn up any source down to ∼23 AB mag. Without more detections in the radio or at other wavelengths, it seemed unlikely that the nature of J1755−2527 could ever be resolved.

In this paper, we present new radio observations (spanning frequencies from 154 MHz to 3.1 GHz) in which J1755−2527 was re-detected, confirming that it is indeed an LPT with a period of ∼1.16 h. In Section 2, we describe the observations themselves, some of which were taken as part of independent surveys, and some of which were taken as dedicated follow-up of J1755−2527 once it became apparent that it was still active. In Section 3 we present a timing analysis of the new detections, as well as revised estimates of the dispersion measure (DM) and the scattering time-scale. We also include new polarization detections in which the polarization angle (PA) behaviour differs significantly from the originally detected pulse. In Section 4 we revisit the question of the nature of J1755−2527, arguing in favour of a white dwarf interpretation. The main conclusions are summarized in Section 5.

2 OBSERVATIONS

Pulses from J1755−2527 were detected with the Murchison Widefield Array (MWA; Tingay et al. 2013), the Australian SKA Pathfinder (ASKAP; Hotan et al. 2021), MeerKAT (Jonas &

★ E-mail: sam.mcsweeney@curtin.edu.au

Table 1. Observations summary.

Date range (MJD)	Telescope	Project	ν (MHz)	$\Delta\nu$ (MHz)	Obs. (num. $\times$) length (min)	Number of pulses
59965	ASKAP	SB47253 (original discovery)	887.5	288	12.1	1
59966	MWA	G0060	161.92	15.36	6.7	1
60040	ASKAP	SB49153	887.5	288	12.1	1
60092–60093	MeerKAT	DDT-20230525-DD-01	1284	856	307	4
60463–60563	MWA	G0080	200.32	30.72	16 × 4.9	16
60503	ASKAP	SB63600	887.5	288	12.3	1
60572	MWA	D0042	184.96	30.72	4 × 4.9	4
60587	ATCA	C3363	2100	2048	93.2	2
60592–60602	MWA	D0042	200.32	30.72	17 × 4.9	17
60602	MeerKAT	DDT-20241015-NH-01	812.8	495.3	10	1

MeerKAT Team 2016), and the Australia Telescope Compact Array (ATCA; Wilson et al. 2011), all radio interferometers capable of imaging. A summary of all the observations containing pulse detections included in this work is presented in Table 1.

In this section, we describe how each telescope was used to generate dynamic spectra of J1755−2527.

2.1 MWA

The MWA, in its Phase II 'extended' configuration (Wayth et al. 2018), was used to scan the Galactic plane for transient radio sources under the 'Galactic Plane Monitor', project code G0080. These observations were conducted over 2022 June–September, and 2024 June–2025 March. Relevant to this work, the region $285^\circ < l < 65^\circ$, $|b| < 15^\circ$ was scanned on a bi-weekly cadence at 185–215 MHz in both 2022 June–September and 2024 June–September (see Methods of Hurley-Walker et al. 2023, a full description will be released by Hurley-Walker et al. in preparation).In this region, the root-mean-squared noise level on the processed 4-s time-scale is $\sim$80 mJy beam^{-1}. Among several detection methods (described in full by Horváth et al., submitted), a convolution filter is employed to extract pulse-like signals. In 2022 June–September, no pulses from J1755−2527 were detected, but in 2024 June, the source was blindly detected as a $\sim$70-s-wide pulse whose peak flux density was 665 mJy.

Subsequent to its redetection, we commenced a Director's Discretionary Time (DDT) campaign under project code D0042, to obtain further observations, adjusting the frequency from 200.32 to 184.96 MHz for some of the observations to attempt to improve measurements of its DM. Time of arrival (ToA) predictions for the DDT observations were made using a preliminary ephemeris derived from the GPM detections, which, by virtue at being at the same or similar frequencies, absorbed the delays due to dispersion and scattering into the 'PEPOCH' term.

We imaged both the 2024 GPM data and the follow-up DDT data at the location of J1755−2527 using WSCLEAN (Offringa et al. 2014), masking J1755−2527 itself, forming a deep model of the sky for each observation. After subtracting this from the visibilities, we phase-rotated to J1755−2527, and averaged the baseline data to produce a dynamic spectrum.

An additional MWA observation made as part of the MWA Interplanetary Scintillation (IPS) Survey, project code G0060, taken just 1 d after the original ASKAP pulse, was found to have J1755−2527 in the field of view. The pulse was detected as a point source in the image formed from the third of three adjacent 200-s, near-Sun observations (30° elongation). In this paper we present both the second and third observations (6.7 min total), in order to make the contrast between detection and non-detection more visible in the light curve formed by averaging over the 15.36-MHz subband, using 10-s time bins. A full description of how MWA IPS observations are scheduled and processed can be found in section 2 of Morgan, Chhetri & Ekers (2022), but the essential details are summarized here. The observations are taken over two equal bands of frequency, centred on approximately 80 and 160 MHz. For this study, only the upper band has been processed. The observations were self-calibrated against a sky model based on the GLEAM survey (Hurley-Walker et al. 2017) using MWA_HYPERDRIVE,[1] and then imaged using WSCLEAN. Further details of the imaging of IPS observations since the first data release can be found in Waszewski et al. (2025, and references therein).

2.2 ASKAP

Paper I presented an exhaustive search of the ASKAP data available at the time of writing, comprising 60 h of data, and yielding only a single detection of J1755−2527 (in Scheduling Block ID 47253). Subsequent to the writing of Paper I, a further search for transient signals in ASKAP data was performed (SBID 63600) in which J1755−2527 produced a detectable pulsation.

With the re-detection of the source in the MWA data, and the calculation of an ephemeris (Section 3), we re-reduced the data in which we would predict that J1755−2527 would appear. We made one further detection, in SBID 49153, at a relatively low significance ($\sim 5\sigma$). We followed a similar procedure as the above to generate dynamic spectra for each of the observations, using a minimum baseline length of 500 m to suppress uncleaned Galactic diffuse emission.

2.3 MeerKAT

MeerKAT observations were undertaken on 2024-10-19, under proposal code DDT-20241015-NH-01 and capture block 1729341386, using the UHF band spanning 544–1088 MHz. As well as correlator observations undertaken at 2-s/132.812-kHz resolution, we also employed the Pulsar Timing User Supplied Equipment (PTUSE; Bailes et al. 2020) in search mode, using 37.45-μs sampling. The observation included typical bandpass, polarization, and phase calibrators, as well as phase-up and test pulsar observations. J1755−2527 was tracked from 13:54:36 to 14:04:35 UTC.

The correlator data were calibrated using the standard SARAO SDP calibration pipeline, and imaged using WSCLEAN. We formed a deep model of the sources within the primary beam, excepting

[1] https://github.com/MWATelescope/mwa_hyperdrive

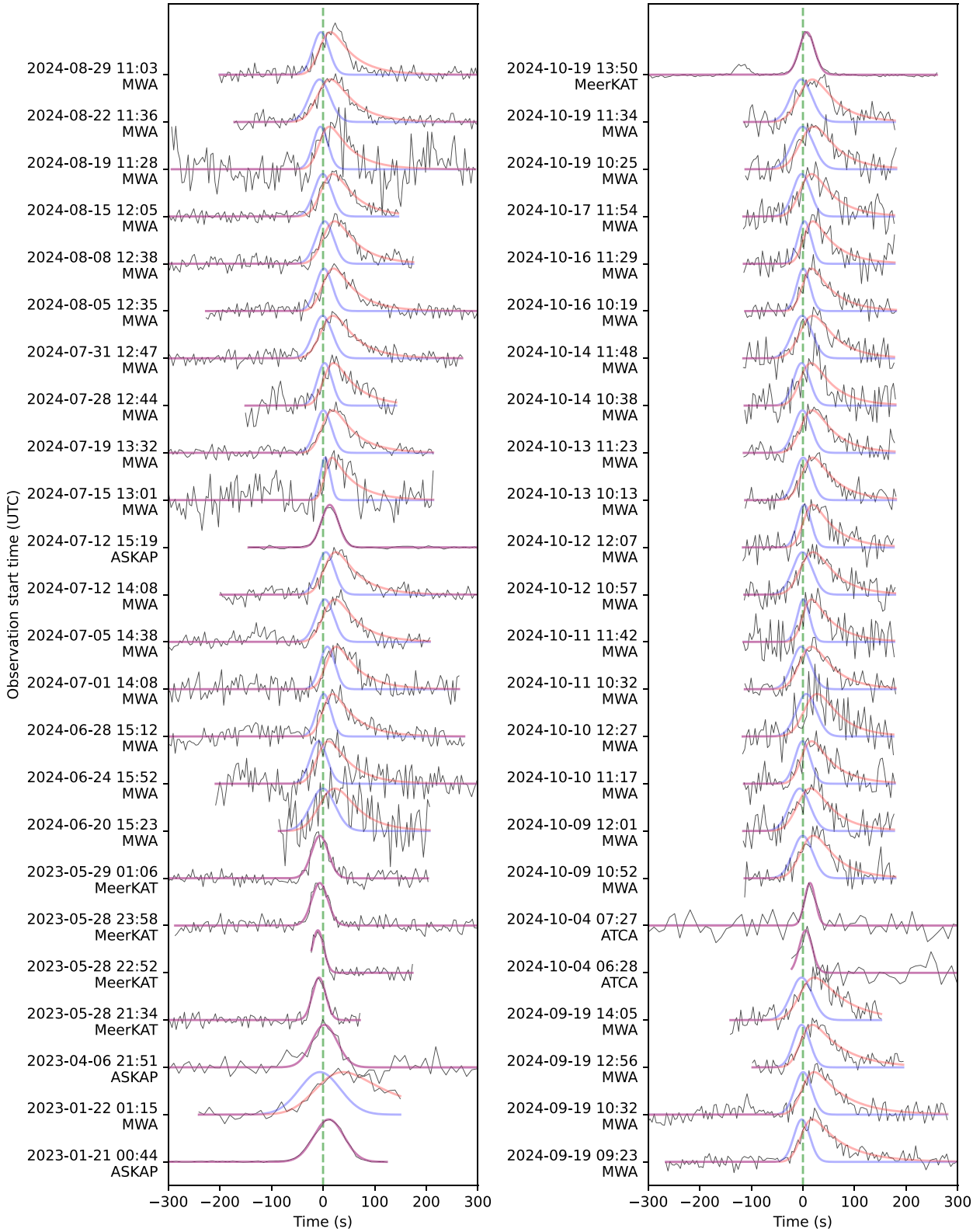

Figure 2. Pulsestack of barycentred dedispersed profiles from the ephemeris. The dashed green vertical line marks zero phase. Baselines have been fitted and subtracted from each light curve. The red curves are fits of the normalized pulses to equation (1), and the blue curves are the inferred Gaussian pulses without scattering, also normalized (see the main text for details).

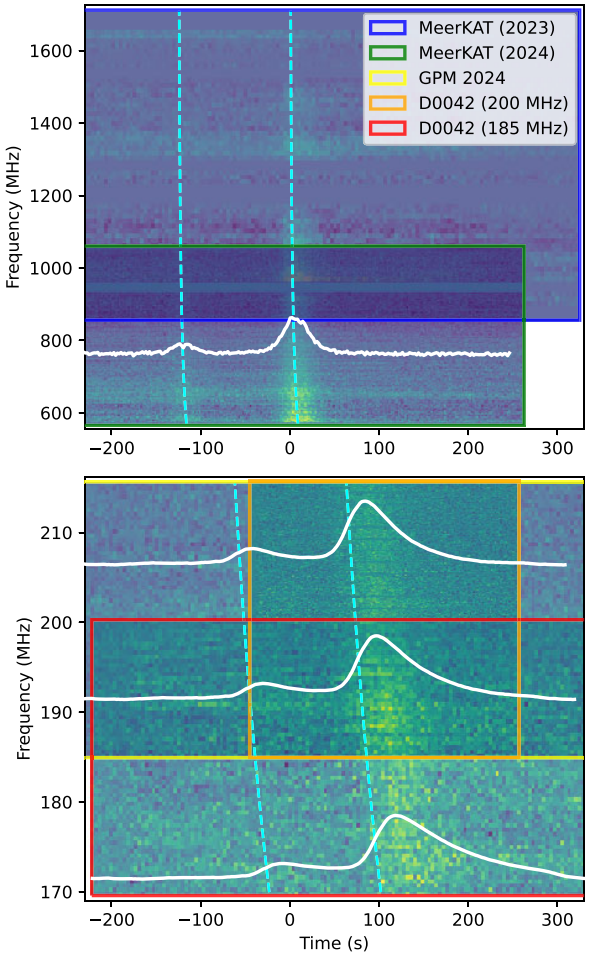

Figure 1 Stacked (semitransparent) dynamic spectra, where each rectangle indicates the observing campaign whose spectra were barycentred and folded according to the ephemeris. The spectra have not been dedispersed, but the cyan dashed lines indicate where the two components seen in the MeerKAT (2024) observation would appear due to dispersion. The white curve in the top panel is the dedispersed profile of the MeerKAT (2024) observation, and the white curves in the bottom panel are the same profile subjected to scattering with $\tau_{\rm sc} = \tau_{\rm sc,1\,GHz}(\nu/1\,{\rm GHz})^{-4}$ at frequencies 175, 195, and 210 MHz, where $\tau_{\rm sc,1\,GHz} = 70$ ms.

J1755−2527, and subtracted this from the visibilities. We then averaged the visibilities, excluding all baselines shorter than 150 m, to produce a dynamic spectrum of the source, shown in Fig. 1. We used the source-finding software AEGEAN (Hancock, Trott & Hurley-Walker 2018) to obtain an updated position of 17:55:34.87(2) −25:27:49.9(4). As in Paper I, we find no coincident sources in either optical or near infrared at the same location (see Appendix A).

We also re-imaged the original 2023-05-28 *L*-band MeerKAT observation described in Paper I, which was taken under project code DDT-20230525-DD-01 under capture block 1685306788. We performed a similar processing of the data, and identified four pulses with ToAs consistent with an ephemeris derived from the other data. The folded and stacked dynamic spectra are shown in Fig. 1.

2.4 ATCA

Following its re-detection in the ASKAP data, follow-up observations were conducted at L/S bands with the ATCA telescope under the project code C3363 (P.I: Tara Murphy). J1755−2527 was observed once on 2024 October 4, for a total of 1.5 h, and again on 2024 October 12, for a total of 2.4 h. At the beginning of each observation, 1934−638 was used to calibrate the bandpass, and during the observations, 1748−253 was used as a phase calibrator. Data were flagged, calibrated, and imaged using standard recipes from the COMMON ASTRONOMY SOFTWARE APPLICATIONS package (CASA; CASA Team 2022). The resulting sky model was subtracted from the visibilities (excluding the source of interest). These model-subtracted visibilities were phase-centred on the J1755−2527 and averaged over the baselines to produce the dynamic spectra.

We identified two faint pulses (4–5σ; see Table C1) in the observation taken on 2024 October 4. However, observations taken on 2024 October 12 did not yield any pulses (at 3σ level). We inspected the data around the expected ToA (using equation 3) but did not find any pulses. The instantaneous noise level, per 10 s integration time bin, around the expected ToAs is close to 1 mJy beam^{-1}. If pulse-to-pulse flux density variations, similar to ones observed in MWA data (Table C1), also occur at L/S band, then even a factor 1.5–2 variation can be sufficient to explain the detection of pulses on 2024 October 4 and the absence of pulses on 2024 October 12, given that the source is faint at higher frequencies.

3 ANALYSIS AND RESULTS

3.1 Pulse morphology

All observed pulses consist of a single burst, approximately Gaussian in shape, with the sole exception of the MeerKAT pulse observed on 2024 October 19, for which two bursts were observed separated by ∼125 s. Generally, the low-frequency (MWA) pulses tend to

(i) be wider than their higher frequency counterparts,
(ii) exhibit an asymmetry resembling a scatter-broadened tail, and
(iii) have minimal pulse-to-pulse morphological variation.

The low-frequency asymmetry is consistent with a scattering time-scale of a few tens of seconds at MWA frequencies, which scales to a few tens of milliseconds at 1 GHz. This is in broad agreement with the model predictions of NE2001 ($\tau_{\rm sc,1GHz} = 66$ ms) and YMW16 ($\tau_{\rm sc,1GHz} = 75$ ms) at the source's location assuming the DM value of 710 pc cm^{-3} reported in Paper I.

To account for the asymmetry, we fit exponentially modified Gaussians to each pulse with the form

$$\mathrm{emg}(t) = A\frac{\sigma}{\tau}\sqrt{\frac{\pi}{2}}\exp\left(-\frac{1}{2}\left(\frac{t-\mu}{\sigma}\right)^2\right)\mathrm{erfcx}\left(\frac{1}{\sqrt{2}}\left(\frac{\sigma}{\tau}-\frac{t-\mu}{\sigma}\right)\right), \quad (1)$$

where $\mathrm{erfcx}(X) = \exp(X^2)\,\mathrm{erfc}(X)$ is the scaled complementary error function; A, μ, and σ are the height, location, and scale of an unscattered Gaussian pulse; and the scattering time-scale was fixed at

$$\tau(\nu) = 0.07\left(\frac{\nu}{\rm GHz}\right)^{-4}\ {\rm s}, \quad (2)$$

according to each observation's centre frequency. A pulse stack containing all observed pulses and the corresponding unscattered pulses derived from the fits is shown in Fig. 2.

For the MeerKAT pulse with two components, we fit only the brighter component. We checked the higher time resolution PTUSE data for finer substructure, but did not find anything smaller than the components that can be seen in Fig. 2.

Table 2. Timing ephemeris for J1755−2527.

Parameter	Value
Period (s)	4186.3285 ± 0.0002
PEPOCH (MJD)	59965.03792 ± 0.00003
DM (pc cm^{-3})	733 ± 22
$\tau_{\rm sc,1GHz}$ (s)	$\sim$0.07
Spindown rate (s s^{-1})	$(-10 \pm 92) \times 10^{-12}$

3.2 Timing solution

Since the large scattering time-scale at low frequencies significantly distorts the pulse shapes, common methods for defining ToAs can potentially result in systematic errors of up to tens of seconds, as discussed in detail in Appendix B. These systematic errors set up a degeneracy between DM and scattering time-scales that is not easily disambiguated.

This is demonstrated in Fig. 1, which shows stacked MWA and MeerKAT spectra. The cyan lines show the expected ToAs across the whole observed frequency range if one assumes only a DM measured at higher frequencies, where scattering is negligible. The scattering predicted by Galactic electron density models, however, is sufficient to account for the apparent extra delay, as is evidenced by the relatively good agreement with the modelled unscattered pulses with the expected ToAs derived from the ephemeris, illustrated in the pulsestack shown in Fig. 2.

We therefore identified the ToAs with the μ parameter in the fits given in equation (1), which represents the location of the assumed Gaussian pulse before scattering. Because the scattering time-scale could not be reliably measured for all individual pulses, we obtained ToAs by assuming a fixed scattering time of $\tau_{\rm sc,1GHz} = 70$ ms.

These ToAs were then barycentred and fit for both period and DM, resulting in the values given in Table 2. The residuals are presented in Fig. 3 and Table C1, along with other fitted properties of the pulses. We also tried fitting a timing model that included a spin-down/up parameter (fixing the DM to 733 pc cm^{-3}), and found that it was consistent with zero. However, owing to the recent discovery that the LPT CHIME/ILT J1634+44 is spinning up ($\dot{P} = (-9.03 \pm 0.11) \times 10^{-12}$ s s^{-1}; Bloot et al. 2025; Dong et al. 2025), we report the fitted period derivative value of $(-10 \pm 92) \times 10^{-12}$ s s^{-1} instead of only providing an upper limit for the spin-down.

The variability of the pulse brightness, coupled with the fact that none of our detections were simultaneous at multiple telescopes, prohibit a direct spectral index measurement. We note, however, that the fitted peak flux densities of the ASKAP and MeerKAT pulses are broadly consistent with the MWA flux densities at nearby epochs if an approximate spectral index of $\alpha = -2.0$ is assumed. The bottom panel of Fig. 3 shows the peak flux densities scaled to 1 GHz under this assumption, revealing a relatively slow change of

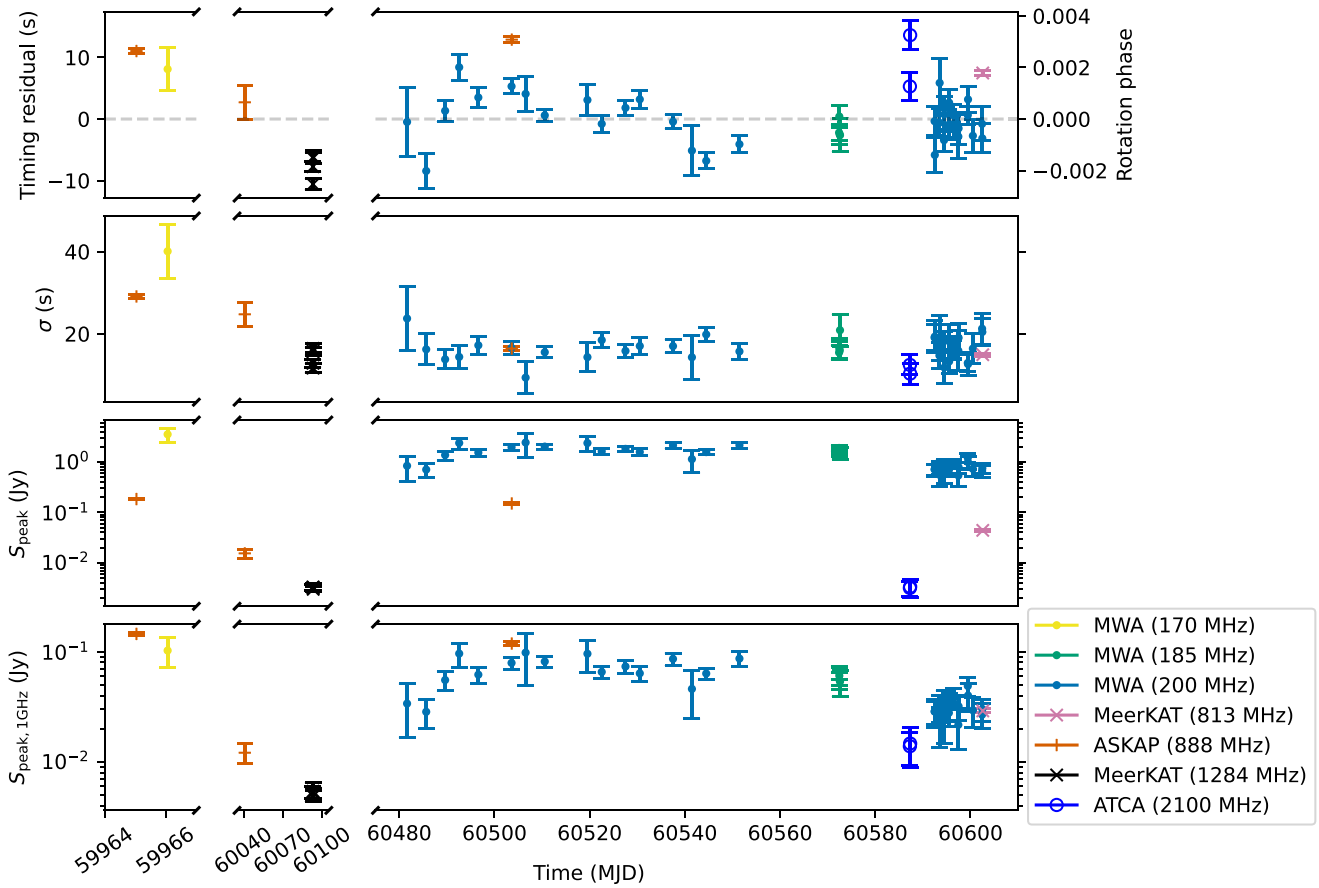

Figure 3. Timing residuals (top panel) and other pulse properties derived from the fits of equation (1) to the individual light curves (second and third panels). The peak flux, $S_{\rm peak}$, equivalent to the A parameter in equation (1), is the peak flux of the modelled unscattered pulse. The bottom panel displays $S_{\rm peak,1GHz} = S_{\rm peak}(\nu/{\rm GHz})^{-\alpha}$, where $\alpha = -2$ has been assumed. Notable features of interest include the relative brightness of the early 2023 detections (leftmost two points), and the relative stability of the pulse fluences (and pulse morphology) of the MWA detections in the time range $60480 \leq {\rm MJD} \leq 60580$. See Table C1 for the values shown in this figure.

the pulses' brightness, not unlike GLEAM-X J1627−5235 (Hurley-Walker et al. 2022). The in-band spectral index measurement of $\alpha = -3.1$ reported for the 2023 ASKAP pulse (Paper I), if consistent across the timespan of our observations, implies a turnover or spectral curvature at intermediate frequencies (perhaps comparable with GPM 1839−10; Hurley-Walker et al. 2023).

The measured DM of 733 ± 22 pc cm^{-3} is slightly higher than, but still consistent with, the in-band measurement of 710^{+200}_{-180} pc cm^{-3} given in Paper I. Because we have not attempted to simultaneously fit for both DM and scattering time-scale, there will remain some small systematic error on this reported DM measurement. Note, in particular, that the YMW16 and NE2001 models predict a slightly longer scattering time-scale than the 70 ms that we have assumed throughout this work. Breaking the degeneracy is possible in principle with a higher S/N average profile than what is achievable with the current data set.

For planning observations of J1755−2527 at low frequencies ($\lesssim$ 300 MHz), care should be taken to incorporate scattering into the predicted ToAs. The Nth pulse since PEPOCH is predicted to arrive at the Solar system barycentre at

$$\mathrm{MJD} = \mathrm{PEPOCH} + N\,P + \Delta t_{\mathrm{DM}}(\nu) + \Delta t_{\mathrm{sc}}(\nu), \tag{3}$$

where PEPOCH and the period, P, are given in Table 2,

$$\Delta t_{\mathrm{DM}}(\nu) = 4148\,\mathrm{s}\left(\frac{\mathrm{DM}}{\mathrm{pc\,cm^{-3}}}\right)\left(\frac{\nu}{\mathrm{MHz}}\right)^{-2} \tag{4}$$

is the usual dispersion attributed to the interstellar medium, and

$$\Delta t_{\mathrm{sc}}(\nu) = -\sqrt{2}\sigma\,\mathrm{erfcx}^{-1}\left(\frac{\tau(\nu)}{\sigma}\sqrt{\frac{2}{\pi}}\right) + \frac{\sigma^2}{\tau(\nu)} \tag{5}$$

is the amount that the *peak* of the observed pulse is delayed by scattering. When calculating this quantity, we recommend using $\sigma = 15$ s, a typical value for low-frequency pulses (see Fig. 3). At frequencies above 300 MHz, $\tau(\nu) \ll \sigma$, and the delay due to scattering, which asymptotically behaves like $\Delta t_{\mathrm{sc}}(\nu) \sim \tau$, can be safely neglected. At frequencies below 150 MHz, the asymptotic behaviour

$$\Delta t_{\mathrm{sc}}(\nu) \sim \sigma\sqrt{\ln\left(\frac{\tau^2}{2\pi\sigma^2}\right)} + \frac{\sigma^2}{\tau} \tag{6}$$

is accurate to within a few seconds. At intermediate frequencies (150 MHz $\lesssim \nu \lesssim$ 300 MHz), equation (5) should be used directly.

3.3 Polarization

No significant linear or circular polarized emission was detected in the 2023 MeerKAT pulses. This is likely due to low S/N coupled with the source not being centred in the beam. Much more careful imaging analysis would be needed to obtain reliable measurements or limits on the polarized components of those pulses. We also find no significant polarized emission from the ATCA pulses.

Given J1755−2527's rotation measure (RM) of ∼961 rad m^{-2} (as reported in Paper I), linearly polarized emission would undergo several tens of degrees of rotation per 40 kHz channel of the GPM observations, and therefore be somewhat depolarized. To offer the best chance of detecting polarized emission, the MWA DDT observations between MJD 60592 and 60602 (see Table 1) were taken with a frequency resolution of 10 kHz, which would result in only 12° of rotation per channel at 200 MHz. We report no significant linearly polarized emission after de-Faraday rotating[2] these observations at −961 rad m^{-2}. We also report that no significantly circularly polarized emission was seen in any MWA observation.

The three sufficiently bright pulses for which we report significant polarization are (1) the original 2023 ASKAP pulse, whose polarization has already been discussed at length in Paper I, (2) the 2024 ASKAP pulse, and (3) the 2024 MeerKAT pulse. We applied the parallactic angle correction to the MeerKAT data, as this had not already been applied during upstream processing.

The high S/N of each time bin allowed us to test whether the RM was consistent across each pulse. We therefore performed a joint fit of the Stokes Q and U spectra of each time bin to

$$Q(\nu) = \mathrm{Re}(\mathcal{L}(\nu)), \quad U(\nu) = \mathrm{Im}(\mathcal{L}(\nu)), \tag{7}$$

where

$$\mathcal{L}(\nu) = L_{1\,\mathrm{GHz}}\left(\frac{\nu}{1\,\mathrm{GHz}}\right)^{\alpha_L} e^{2i(\mathrm{RM}\,\lambda^2+\psi_0)}, \tag{8}$$

$L_{1\,\mathrm{GHz}}$ is the flux density of the linearly polarized component at 1 GHz, α_L is its spectral index, RM is the rotation measure, $\lambda = c/\nu$ is the wavelength, and ψ_0 is the intrinsic PA. The RMs and spectral indices of these fits are shown in the top two rows of panels of Fig. 4.

We found that the RM derived for the MeerKAT pulse had the opposite sign, but similar magnitude, to the ASKAP pulses, which is most likely due to a different sign convention being used within the two telescopes' pre-processing software. The agreement presented in Fig. 4 was achieved by first negating Stokes Q in the MeerKAT data. Any reflection in the Q-U plane (e.g. Q ↔ −Q, U ↔ −U, or Q ↔ U) will achieve a similar correction to the sign of the RM, but different choices will introduce different offsets to the PA. Because of this, the MeerKAT PA values should not be directly compared with the ASKAP values. The most likely scenario, however, is that the MeerKAT values include an arbitrary offset of $n \times 45°$, for some integer n.

In all cases, the magnitude of the fitted RM was within a few rad m^{-2} of the value originally derived for the 2023 ASKAP pulse in Paper I. The RM appears to decrease slightly over the course of the 2023 ASKAP pulse, and *increase* slightly over the course of the two 2024 MeerKAT components; however, all values are consistent with a constant RM across all three pulses. The per-pulse weighted averaged values (with weighting proportional to the Stokes I profile) are 962 ± 1 rad m^{-2} (2023 ASKAP), 965 ± 2 rad m^{-2} (2024 ASKAP), and 962 ± 2 rad m^{-2} (2024 MeerKAT). The spectral index of the linear component, α_L, is similarly consistent, with averages value of -2.1 ± 0.4 (2023 ASKAP), -3.0 ± 0.6 (2024 ASKAP), and -1.9 ± 0.5 (2024 MeerKAT).

Each pulse was de-Faraday rotated with the weighted average RM given above, to derive the linear polarization profile and the PA evolution across the pulses. For the 2023 ASKAP pulse, we recover the 'S'-shaped PA curve discussed at length in Paper I in the context of the rotating vector model (RVM). Contrastingly, the PA curve of the 2024 ASKAP pulse is flat (across five 10-s bins), and that of the 2024 MeerKAT pulse is curved, but not in an RVM-like way.

4 DISCUSSION

After accounting for dispersion and scattering effects, the timing analysis of J1755−2527 confirms its status as an LPT, as originally

[2]On account of the possible sign ambiguity of the reported RM, we also tried de-Faraday rotating the MWA observations at 961 rad m^{-2}.

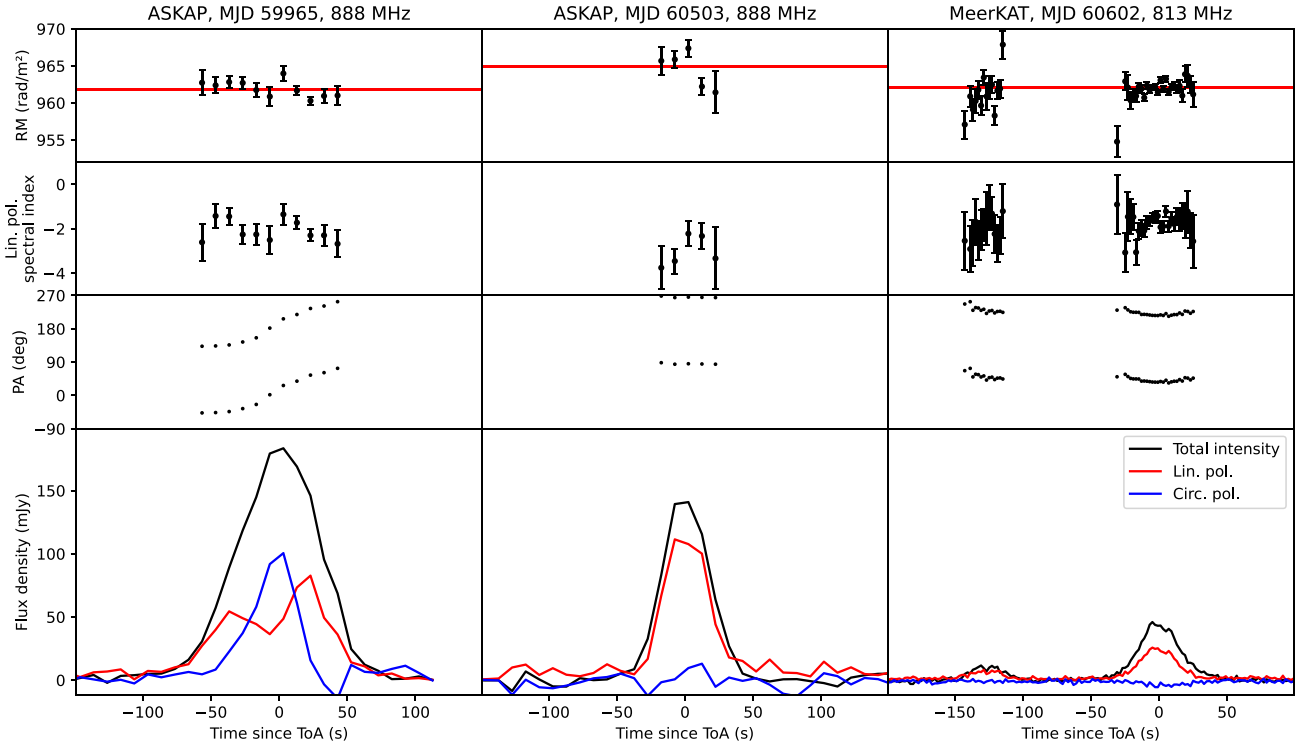

Figure 4. Polarization of the 2023 and 2024 ASKAP pulses (left and middle) and the 2024 MeerKAT pulse (right). The top two rows show the RM and $\alpha_{\rm lin}$ parameters fitted to equation (7) for each time bin independently. Only bins for which the uncertainty on $\alpha_{\rm lin}$ is less than 1.4 are shown, a threshold that was found to cleanly eliminate off-pulse bins. The weighted average RMs for each pulse are indicated by the horizontal red lines. The PAs and light curves shown in the bottom two rows of panels were produced using only the average RM for the respective pulse.

conjectured in Paper I. It has the fifth largest period (∼1.16 h) of published LPTs to date, after ASKAP J1839−0756 (6.45 h; Lee et al. 2025), GLEAM-X J0704−37 (2.92 h; Hurley-Walker et al. 2024; Rodriguez 2025), ILT J1101+5521 (2.09 h; Ruiter et al. 2025), and GCRT J1745−3009 (1.28 h; Hyman et al. 2005).

With the timing solution in hand, we can explore the efficacy of the original follow-up campaign described in Paper I. Assuming J1755−2527 remained at a similar brightness (see Fig. 3), it should have been detected in two ASKAP observations (2023 April 6 and 2023 October 18) and a few dozen times throughout the MWA's 2022 GPM run (2022 June 2 to 2022 September 8). More careful cleaning and imaging of the 2023 April 6 ASKAP observation revealed a low-S/N pulse, at the time predicted by the ephemeris, which is presented in Figs. 2 and 3. There are also three observations in the earliest part of the 2024 GPM run (one on 2024 June 2 and two on 2024 June 10) in which no pulse was observed. However, pulses were detected just 10 d later on 2024 June 20 (the first of the MWA 200 MHz points in Fig. 3), and at each epoch thereafter whenever the MWA was observing in J1755−2527's direction when a pulse was due to arrive.

In contrast, the ATCA observation taken on 2024 October 12 did not yield any detections (out of four possible predicted ToAs that occurred during that observation). This is despite the fact that pulses were detected with ATCA just 8 d prior with a similar instantaneous noise level (∼1 mJy), as well as the fact that pulses were detected at the MWA within 24 h of the ATCA observation (none of the MWA observations were coincident with the ATCA observation). However, even a modest amount of pulse-to-pulse variability would allow for the possibility that the pulses during the 2024 October 12 were present, but fell below the detection threshold of ATCA.

We conclude therefore that J1755−2527 is intermittent with active periods lasting of the order of months, and that the most recent activity period fortuitously started shortly after the start of the 2024 GPM observation run. The entire set of observations presented in this work, spanning from 2023 to 2024, may represent two or three different activity windows. This is reminiscent of the behaviour of GLEAM-X J162759.5−523504.3, which was 'on' in 2018 January, 'off' in Feburary, and 'on' again in March (Hurley-Walker et al. 2022). The reappearance of J1755−2527 suggests the possibility that other known intermittent LPTs (like GLEAM-X J162759.5−523504.3 and GCRT J1745−3009) may eventually do likewise.

As noted in Paper I, optical follow-up of J1755−2527 is hampered by its position within the Galactic plane ($b = -0.12°$) and the associated extinction. Inferring the nature of this system (white dwarf versus neutron star, isolated versus binary) from the radio pulses alone is challenging, until either the population of LPTs is better understood as a whole, or some other property of the radio signal (e.g. intermittency, polarization) can be linked to the system properties.

J1755−2527's period and duty cycle are not dissimilar to ILT J1101+5521 and GLEAM-X J0704−37, both thought to be WD + MD binary systems (Fig. 5), suggesting the possibility that J1755−2527 is also such a system. Notably, its period of ∼1.16 h would make it shorter than the minimum known orbital period of 1.3 h for polars (Gänsicke et al. 2009; Schwope 2025). This makes it an interesting test bed for the possibility that LPTs with

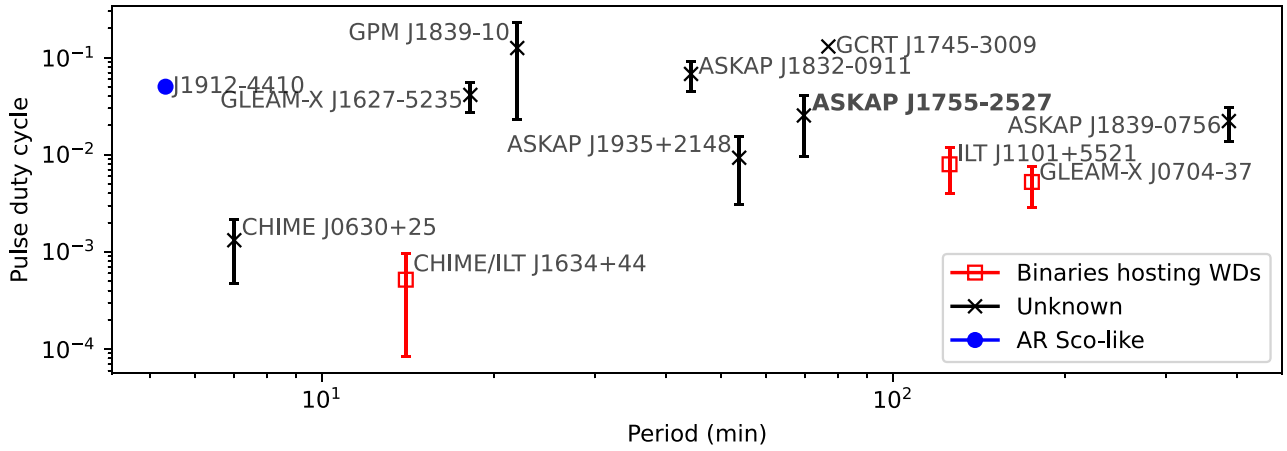

Figure 5. Duty cycle versus radio pulse period for various long-period radio emitters (Hyman et al. 2005; Hurley-Walker et al. 2022, 2023; Caleb et al. 2024; Wang et al. 2025; Lee et al. 2025; Ruiter et al. 2025). The duty cycles are derived from the reported pulse widths for LPTs, which are compared to the range of the fitted unscattered pulse widths of J1755−2527 at 10 per cent of the peak. AR Sco (Marsh et al. 2016; Stanway et al. 2018) and other sources without well-defined duty cycles or periods (e.g. Wang et al. 2021, and references therein) are not included on this plot.

different periods represent different stages of WD + MD binary evolution.

There is as yet no clear consensus on whether LPTs represent one class or multiple classes of system (e.g. Rea et al. 2024). However, the recent confirmation of AR Scorpii (Marsh et al. 2016), J1912−4410 (Pelisoli et al. 2023), and SDSS J230641.47+244055.8 (Castro Segura et al. 2025) as white dwarf pulsars and ILT J1101+5521 and GLEAM-X J0704−37 as WD + MD systems (Rodriguez 2025; Ruiter et al. 2025), and CHIME/ILT J1634+44 as a binary hosting a white dwarf (possibly two, Bloot et al. 2025; Dong et al. 2025) raise the intriguing possibility that other LPTs may also be radio-emitting white dwarf pulsars at various stages of evolution (Schreiber et al. 2021, Horváth et al. submitted).

In this view, the intermittency of these systems have several possible explanations. The limited orbital phase range in which J1912−4410's radio pulses were observed suggests that the geometric configuration is important in the observability of radio pulsations; 'missing' pulses may simply occur at unfavourable orbital phases. This is readily testable with long-term monitoring – this kind of intermittency will have the same periodicity as the orbit itself.

Interestingly, systems with spin-orbital (or beat-orbital) resonances of, e.g. 2:1 or 3:1, would be indistinguishable from systems in 1:1 resonances if pulses can only be observed within a limited orbital phase range. We therefore raise the possibility that the coincidence of the observed radio periodicities of ILT J1101+5521 and GLEAM-X J0704−37 with their spectroscopically confirmed orbital periods does not necessarily imply that they are 1:1 systems.

In a similar vein, systems in which the spin-orbit (or beat-orbit) ratios are *close to* small-integer ratios, or, similarly, systems in which precession of the WD is significant, will exhibit an extra beating effect in which an orbitally induced intermittency is aliased to a much lower frequency. The month-long time-scale of the intermittency of J1755−2527, and possibly even GLEAM-X J1627−5235, may be of this kind; much longer term monitoring is needed to confirm or refute this.

Another possibility is that radio emission is only observed when the companion produces dense enough particle outflows, in the form of winds, to activate the emission mechanism in the vicinity of the WD. This may be the case, for example, for GLEAM-X J0704−37, whose spectroscopically detected Hα emission is associated with the M-dwarf, and which may come from its stellar wind (Rodriguez 2025). Such outflows can last for months (Wood et al. 2021), and would not be periodic. We also note that the intermittency and varying polarization properties of J1755−2527 (and other LPTs) may be explained by changes in the local plasma environment (Rose et al. in preparation). If intermittency is of this kind, then the observed activity windows will be similarly aperiodic, or quasi-periodic. Again, long-term monitoring can help distinguish between these scenarios.

5 SUMMARY

We have shown that J1755−2527 is in fact an LPT, as conjectured in Paper I). Its period of ∼1.16 h is slightly shorter than the minimum known orbital period of optically confirmed polars, marking it as an interesting case study in the context of Rodriguez's (2025) suggestion that 'short'-LPTs and 'long'-LPTs may correspond to different classes of CVs.

A timing solution has been presented (equation 3), which includes a term to account for scattering at low frequencies ($\lesssim$ 300 MHz). Without it, ToA predictions may be early by up to several tens of seconds, which is a sizeable fraction of the intrinsic pulse width.

The three higher frequency pulses for which polarimetry was observable exhibited unique single-pulse polarization behaviours. Only the original ASKAP detection exhibited a PA curve that was amenable to being modelled with the RVM; the others show either flat, or slightly concave up PA curves (Fig. 4).

We conjecture that if J1755−2527 is a WD pulsar, its intermittency may be a result of the spin-orbital resonance being near, but not exactly, a small-integer ratio, creating a aliased beating pattern on a time-scale of months. The same explanation may be applied to other LPTs with activity cycles that last of the order of months. An alternative explanation is that the radio emission is drived by particle wind outflows from a main-sequence companion. Long-term monitoring of LPTs will reveal whether the intermittency is periodic, and thus help discriminate between these two scenarios.

ACKNOWLEDGEMENTS

This research is supported by an Australian Government Research Training Program (RTP) Scholarship.

NH-W is the recipient of an Australian Research Council Future Fellowship (project number FT190100231).

This scientific work uses data obtained from Inyarrimanha Ilgari Bundara, the CSIRO Murchison Radio-astronomy Observatory. Support for the operation of the MWA is provided by the Australian Government (NCRIS), under a contract to Curtin University administered by Astronomy Australia Limited. ASVO has received funding from the Australian Commonwealth Government through the National eResearch Collaboration Tools and Resources (NeCTAR) Project, the Australian National Data Service (ANDS), and the National Collaborative Research Infrastructure Strategy. The Australian SKA Pathfinder is part of the Australia Telescope National Facility, which is managed by CSIRO (https://ror.org/05qajvd42). Operation of ASKAP is funded by the Australian Government with support from the National Collaborative Research Infrastructure Strategy. ASKAP and the MWA use the resources of the Pawsey Supercomputing Centre. Establishment of ASKAP, Inyarrimanha Ilgari Bundara, and the Pawsey Supercomputing Centre are initiatives of the Australian Government, with support from the Government of Western Australia and the Science and Industry Endowment Fund. We acknowledge the Wajarri Yamaji People as the Traditional Owners and Native Title Holders of the observatory site.

The MeerKAT telescope is operated by the South African Radio Astronomy Observatory, which is a facility of the National Research Foundation, an agency of the Department of Science and Innovation. Observations made use of the Pulsar Timing User Supplied Equipment (PTUSE) servers at MeerKAT, which were funded by the MeerTime Collaboration members ASTRON, AUT, CSIRO, ICRAR-Curtin, MPIfR, INAF, NRAO, Swinburne University of Technology, the University of Oxford, UBC, and the University of Manchester. The system design and integration was led by Swinburne University of Technology and Auckland University of Technology in collaboration with SARAO and supported by the ARC Centre of Excellence for Gravitational Wave Discovery (OzGrav) under grant CE170100004.

The data base of MWA candidates, and the webapp designed to facilitate manually inspecting them, were developed by Astronomy Data and Computing Services (ADACS) as part of its software support scheme.

SM would like to thank J. Pritchard and E. Lenc for technical discussions regarding the ASKAP data sets included in this paper.

KR thanks the LSST-DA Data Science Fellowship Program, which is funded by LSST-DA, the Brinson Foundation, and the Moore Foundation; their participation in the program has benefited this work.

DATA AVAILABILITY

The raw visibilities for the MWA,[3] ASKAP,[4] and MeerKAT[5] data sets are available via the respective telescopes' data portals. The ATCA[6] data are available on reasonable request to the authors, and will become publicly available from the relevant data portal by 2025 November. The post-imaged dynamic spectra, analyses, and timing analysis data products (ToAs, pulse properties) are publicly available on GitHub.[7]

[3]https://asvo.mwatelescope.org/
[4]https://research.csiro.au/casda/
[5]https://archive.sarao.ac.za/
[6]https://atoa.atnf.csiro.au/

REFERENCES

Bailes M. et al., 2020, Publ. Astron. Soc. Aust., 37, e028
Bloot S. et al., 2025, A&A, 699, A341
Caleb M. et al., 2024, Nat. Astron., 8, 1159
Castro Segura N. et al., 2025, preprint (arXiv:2506.20455)
Chambers K. C. et al., 2016, preprint (arXiv:1612.05560)
de Ruiter I. et al., 2025, Nat. Astron. , 9, 672
Dobie D. et al., 2024, MNRAS, 535, 909
Dong F. A. et al., 2025, ApJ, 988, L29
Gänsicke B. T. et al., 2009, MNRAS, 397, 2170
Hancock P. J., Trott C. M., Hurley-Walker N., 2018, Publ. Astron. Soc. Aust., 35, e011
Hotan A. W. et al., 2021, Publ. Astron. Soc. Aust., 38, e009
Hurley-Walker N. et al., 2017, MNRAS, 464, 1146
Hurley-Walker N. et al., 2022, Nature, 601, 526
Hurley-Walker N. et al., 2023, Nature, 619, 487
Hurley-Walker N. et al., 2024, ApJ, 976, L21
Hyman S. D., Lazio T. J. W., Kassim N. E., Ray P. S., Markwardt C. B., Yusef-Zadeh F., 2005, Nature, 434, 50
Jing W.∼C. et al., 2025, preprint (arXiv:2506.14519)
Jonas J., MeerKAT Team, 2016, in Proceedings of MeerKAT Science: On the Pathway to the SKA. p. 1
Kaiser N. et al., 2010, in Stepp L. M., Gilmozzi R., Hall H. J.eds, Proc. SPIE Conf. Ser. Vol. 7733, Ground-Based and Airborne Telescopes III. SPIE, Bellingham, p. 77330E
Lawrence A. et al., 2007, MNRAS, 379, 1599
Lee Y. W. J. et al., 2025, Nat. Astron. , 9, 393
Marsh T. R. et al., 2016, Nature, 537, 374
Morgan J., Chhetri R., Ekers R., 2022, Publ. Astron. Soc. Aust., 39, e063
Murphy T. et al., 2013, Publ. Astron. Soc. Aust., 30, e006
Offringa A. R. et al., 2014, MNRAS, 444, 606
Pelisoli I. et al., 2023, Nat. Astron., 7, 931
Rea N. et al., 2022, ApJ, 940, 72
Rea N. et al., 2024, ApJ, 961, 214
Rickett B., Johnston S., Tomlinson T., Reynolds J., 2009, MNRAS, 395, 1391
Rodriguez A. C., 2025, A&A, 695, L8
Schreiber M. R., Belloni D., Gänsicke B. T., Parsons S. G., Zorotovic M., 2021, Nat. Astron., 5, 648
Schwope A. D., 2025, A&A, 698, A106
Stanway E. R., Marsh T. R., Chote P., Gänsicke B. T., Steeghs D., Wheatley P. J., 2018, A&A, 611, A66
Team CASA, 2022, PASP, 134, 114501
Tingay S. J. et al., 2013, Publ. Astron. Soc. Aust., 30 , e007
Virtanen P. et al., 2020, Nat. Methods, 17, 261
Wang Z. et al., 2021, ApJ, 920, 45
Wang Z. et al., 2025, Nature, 642, 583
Waszewski A., Morgan J. S., Ekers R., Johnston-Hollitt M., Cheung M. C. M., Bhat N. D. R., Chhetri R., Fu S. C., 2025, Space Weather, 23, e2025SW004342
Wayth R. B. et al., 2018, Publ. Astron. Soc. Aust., 35, e033
Williamson I. P., 1972, MNRAS, 157, 55
Williamson I. P., 1973, MNRAS, 163, 345
Wilson W. E. et al., 2011, MNRAS, 416, 832
Wood B. E. et al., 2021, ApJ, 915, 37

APPENDIX A: MEERKAT LOCALIZATION

Fig. A1 shows the position derived from the MeerKAT detection on MJD 60602.

[7]https://github.com/robotopia/j1755-2527

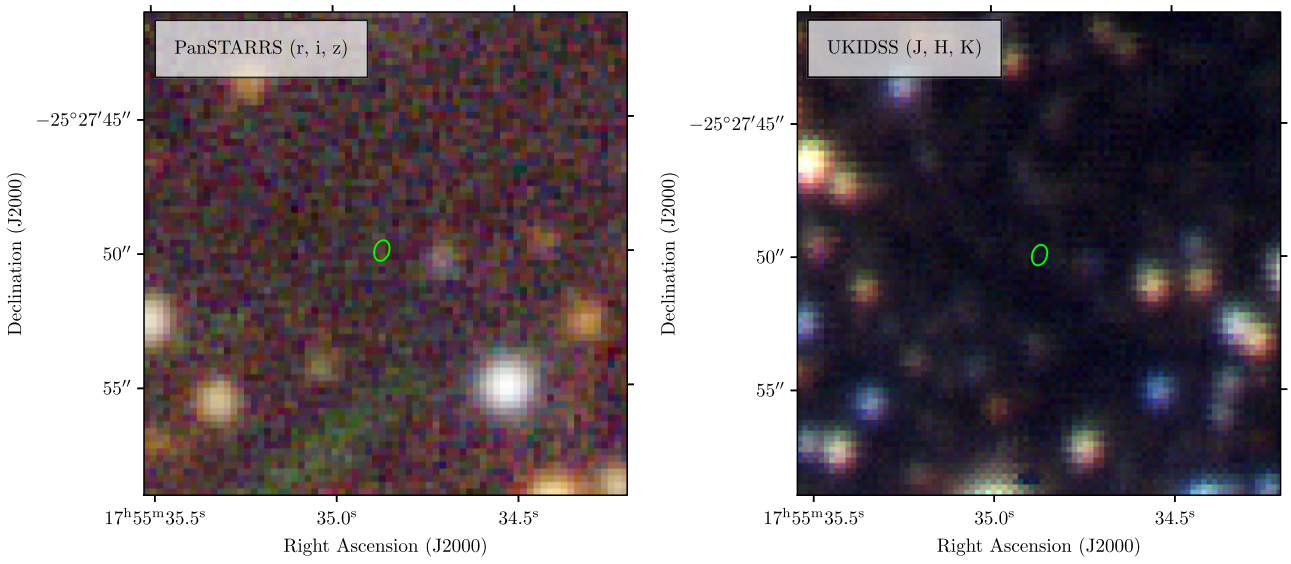

Figure A1. The 1σ positional uncertainty of J1755−2527 derived from the MeerKAT observation taken on MJD 60602 is shown as the green ellipses overlaid on the optical (r, i, z) Panoramic Survey Telescope and Rapid Response System (PanSTARRS; Kaiser et al. 2010; Chambers et al. 2016) image (left panel), and the infrared (J, H, K) United Kingdom Infrared Telescope Deep Sky Survey (UKIDSS; Lawrence et al. 2007) image (right panel).

APPENDIX B: THE EFFECT OF SCATTERING ON TIMING

It can be shown that pulses scatter-broadened by a thin screen[8] will appear to the observer as the original pulse convolved with a one-sided exponential kernel with an associated time-scale τ (Williamson 1972, 1973). For intrinsically Gaussian pulses of scale σ, the result of this convolution is well described by the *exponentially modified Gaussian* (EMG), as given in equation (1).

In the regime $\tau \ll \sigma$, the effect of scattering is negligible and the scattered pulse resembles the original pulse. ToAs can be obtained in the usual way, i.e. using a matched filter 'template' constructed from the average pulse profile.

On the other hand, in the regime $\tau \gg \sigma$, the leading edge of the EMG rises sharply (resembling the error function, erf) and the trailing edge resembles the exponential kernel itself. For this reason, pulse ToAs are typically mapped to the rising edge of highly scattered pulses, which closely approximates the centre of the original unscattered pulse (Jing et al., 2025, and references therein).

In this appendix, we discuss the effect of scattering on measuring a DM from pulse observations if scattering is not taken into account. As will be shown, the effect is most dramatic when $\tau \approx \sigma$, and in the case of wide, highly scattered pulses from LPTs like J1755−2527, can lead to a discrepant DM measurement of several hundreds of pm cm^{-3}.

We consider four methods for defining ToAs:

(1) the position where the leading edge reaches half-maximum (LEHM),

$$\mathrm{emg}(\mathrm{ToA_{LEHM}}) = \frac{1}{2} A \exp\left(-\frac{1}{2}\left(\frac{\mu - t_m}{\sigma}\right)^2\right), \tag{1a}$$

where

$$t_m = \mu - \sqrt{2}\sigma\,\mathrm{erfcx}^{-1}\left(\frac{\tau}{\sigma}\sqrt{\frac{2}{\pi}}\right) + \frac{\sigma^2}{\tau^2}$$

is the mode of the EMG, (2) the inflection point on the leading edge (IPLE),

$$\left.\frac{\mathrm{d}^2 \mathrm{emg}(t)}{\mathrm{d}t^2}\right|_{t=\mathrm{ToA_{IPLE}}} = 0, \tag{1b}$$

(3) the position of the peak of the pulse (PEAK),

$$\mathrm{ToA_{PEAK}} = t_m, \tag{1c}$$

and (4) the maximum of the convolution of the pulse with a Gaussian profile with scale σ (TMPL)

$$\left.\frac{\mathrm{d}}{\mathrm{d}t}\left(\mathrm{emg}(t) * \exp\left[-\frac{1}{2}\left(\frac{t-\mu}{\sigma}\right)^2\right]\right)\right|_{t=\mathrm{ToA_{TMPL}}} = 0. \tag{1d}$$

The last definition is akin to template matching with a high-frequency (negligibly scattered) pulse profile.

None of the methods is entirely accurate in the presence of scattering. We define the errors of the ToAs to be the difference between the measured ToA and the mean of the unscattered pulse,

$$\Delta\mathrm{ToA} \equiv \mathrm{ToA} - \mu. \tag{B2}$$

For LEHM and IPLE, the ToA is measured to be earlier than μ (ΔToA < 0); for PEAK and TMPL, later (ΔToA > 0). ToA$_{\mathrm{LEHM}}$ and ToA$_{\mathrm{IPLE}}$ will perform much better than ToA$_{\mathrm{PEAK}}$ and ToA$_{\mathrm{TMPL}}$ highly scattered pulses ($\tau \gg \sigma$), whereas the converse is true when scattering is minimal ($\tau \ll \sigma$). All methods, however, perform relatively poorly in the intermediate regime when $\tau \approx \sigma$.

We computed numerically (using SciPy's `root` function; Virtanen et al. 2020) the errors for the four ToA types defined above, in the regime around $\tau \approx \sigma$. These are shown in the panel (a) of Fig. B1, normalized to the scale of the pulse, σ. The axis along the top shows the normalized time-scale (inverted, with largest time-scales on the left), while the axis along the bottom shows the equivalent frequencies normalized to ν_s, defined as the frequency at which

[8]Relaxing the assumption of a single thin isotropic screen affects the shape of the scattered pulse in ways that could plausibly affect timing (Rickett et al. 2009), but quantification of this is beyond the scope of this appendix.

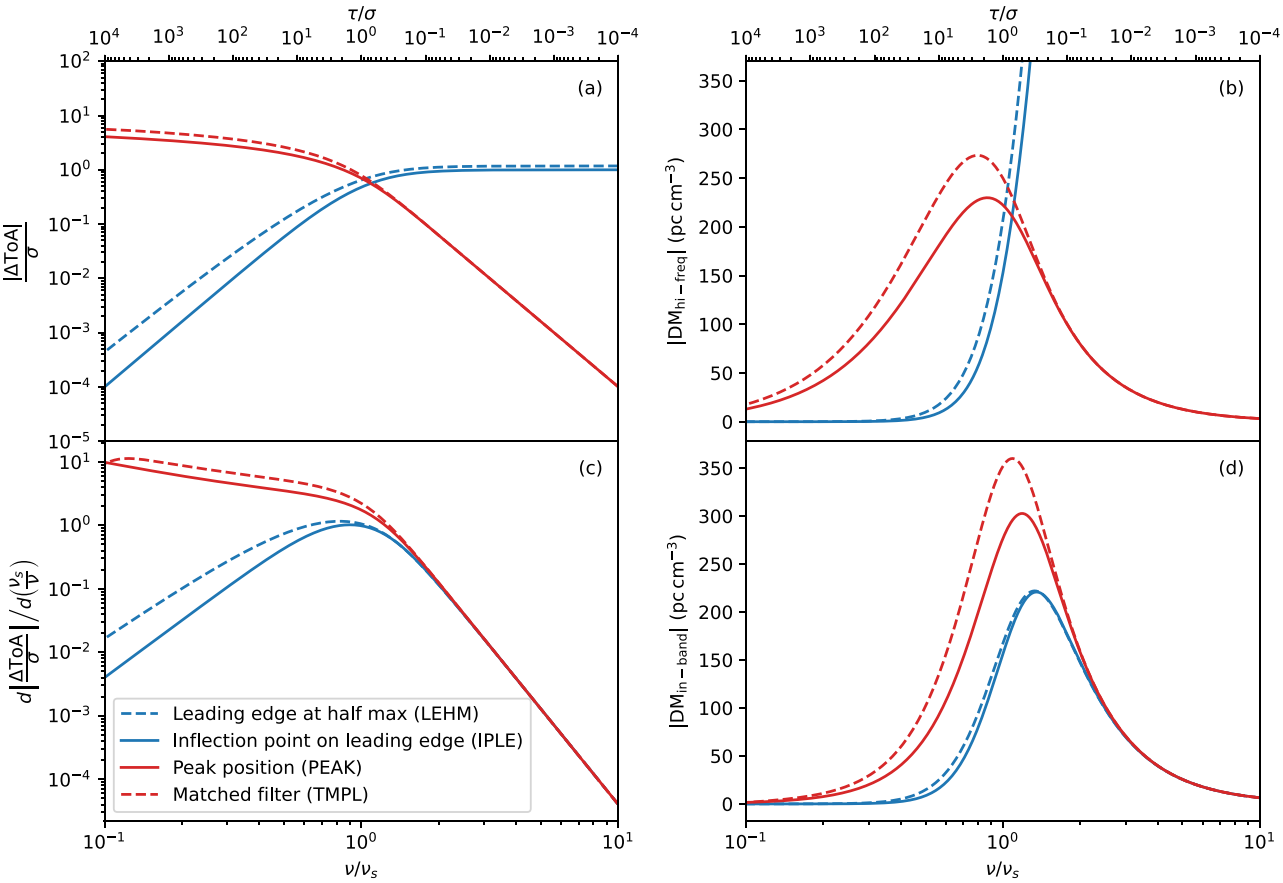

Figure B1. Analysis of DM measurement errors if scattering is not properly taken into account. Panel (a) shows the errors measured for each defined type of ToA, normalized to the scale of the original pulse, σ. In panel (b), the predicted error in DM is shown if the ToA error (compared to a high-frequency ToA measurement) is erroneously attributed to dispersion. Panel (c) shows the rate of change of the ToA error with frequency, and panel (d) shows the error in DM measured if this rate of change (the 'slope' of the pulse across the observed dynamic spectrum) is erroneously attributed to dispersion. In panels (c) and (d), the derived DM errors assume a pulse scale of $\sigma = 25$ s and $\nu_s = 230$ MHz, as estimated for J1755−2527. In all panels, the blue curves indicate *negative* ToA errors (i.e. the measured ToAs are earlier than the pulse's unscattered mean, μ), and the red curves indicate positive quantities.

$\tau = \sigma$. We have assumed a scattering index of −4, such that

$$\frac{\tau}{\sigma} = \left(\frac{\nu}{\nu_s}\right)^{-4}. \tag{B3}$$

A set of ToAs may be converted to DM measurements in two ways: (1) by comparing the ToAs to those measured at much higher frequencies (e.g. with TMPL) where the scattering is known to be negligible, and (2) by measuring the slope of the pulse in the dynamic spectrum (for example, by measuring the ToAs in subbands across the observed frequency range). Panel (c) of Fig. B1 shows the expected slope measurements for the ToA errors given in the panel (a).

In the first case, the ToA error of a pulse measured at frequency ν, if attributed erroneously to the effect of dispersion, will yield a discrepant DM of

$$\Delta\mathrm{DM}_{\mathrm{hi-freq}} \approx \frac{\Delta\mathrm{ToA}\,\nu^2}{\mathcal{D}}. \tag{B4}$$

For the specific case of J1755−2527, for which we estimate $\sigma = 25$ s and $\nu_s = 230$ MHz, consistent with $\tau_{\mathrm{sc,1GHz}} = 70$ ms, the DM error can be as high as a few hundreds of pc cm^{-3}. When using this DM method, it is better to use LEHM or IPLE at frequencies $\nu \lesssim \nu_s$, and PEAK or TMPL for $\nu \gtrsim \nu_s$; however, it should be remembered that LRHM and IPLE will *underestimate* the DM, while PEAK and TMPL will *overestimate* it. All ToA definitions produce sizeable DM errors in the approximate range $\nu_s \lesssim \nu \lesssim 3\nu_s$.

The situation is not much improved for DMs determined via the slope of the pulse across the observed band, for which the scattering-induced slope is mapped to an (erroneous) equivalent DM measurement of

$$\Delta\mathrm{DM}_{\mathrm{in-band}} \approx \frac{\mathrm{dToA}}{\mathrm{d}\nu}\frac{\nu^3}{2\mathcal{D}} \tag{B5}$$

The calculated numbers for J1755−2527 are illustrated in panel (d). For this case, LEHM and IPLE are always preferred to PEAK and TMPL, but the magnitude of the derived DM error is still in the hundreds of pc cm^{-3} at frequencies in the range $\nu_s \lesssim \nu \lesssim 3\nu_s$.

We confirm the order of magnitude of the above results by reporting a measured in-band DM for one of the MWA pulses at 185 MHz, using the TMPL method to measure ToAs in 1.28 MHz subbands from ∼170 to ∼200 MHz, of $\mathrm{DM}_{\mathrm{in-band}} = 1221 \pm 257$ pc cm^{-3}. This exceeds the DM reported in this work by ∼450 pc cm^{-3}, in excess of the prediction shown in panel (d), but consistent within measurement errors.

APPENDIX C: PULSE PROPERTIES

Table C1 provides the fitted parameter values of the pulses shown in Fig. 3.

Table C1. Times of arrival and other fitted pulse properties.

Telescope	Freq (MHz)	ToA (MJD)	S_{peak} (Jy)	σ (s)	Fluence (Jy s)
ASKAP	888	59965.0429346(42)	0.184(5)	29.1(4)	13.4(2)
MWA	170	59966.061584(40)	4(1)	40(7)	358(55)
ASKAP	888	60040.913447(32)	0.015(3)	25(3)	1.0(1)
MeerKAT	1284	60092.8995476(100)	0.0032(4)	12.8(9)	0.104(7)
MeerKAT	1284	60092.947966(10)	0.0033(6)	12(1)	0.10(1)
MeerKAT	1284	60092.996466(11)	0.0032(3)	15.8(9)	0.125(7)
MeerKAT	1284	60093.044919(12)	0.0030(3)	16(1)	0.122(7)
MWA	200	60481.637466(65)	0.8(4)	24(8)	50(11)
MWA	200	60485.658977(33)	0.7(2)	16(4)	29(3)
MWA	200	60489.632266(20)	1.4(3)	14(2)	48(3)
MWA	200	60492.588020(24)	2.4(6)	14(3)	87(7)
MWA	200	60496.609639(18)	1.5(3)	17(2)	67(4)
MWA	200	60503.587085(14)	2.0(2)	17(2)	82(3)
ASKAP	888	60503.6347610(51)	0.151(7)	16.4(5)	6.2(2)
MWA	200	60506.542809(33)	2(1)	9(4)	57(7)
MWA	200	60510.564531(11)	2.0(2)	16(1)	79(3)
MWA	200	60519.528813(29)	2.4(8)	14(4)	86(10)
MWA	200	60522.533028(16)	1.6(2)	18(2)	76(3)
MWA	200	60527.524033(14)	1.8(2)	16(2)	73(3)
MWA	200	60530.528339(16)	1.6(2)	17(2)	68(4)
MWA	200	60537.506042(13)	2.1(3)	17(2)	92(4)
MWA	200	60541.479447(47)	1.1(5)	14(5)	41(6)
MWA	200	60544.483761(15)	1.6(2)	20(2)	79(3)
MWA	200	60551.461625(16)	2.2(3)	16(2)	85(4)
MWA	185	60572.395455(15)	1.9(3)	15(2)	74(3)
MWA	185	60572.443943(21)	1.8(3)	16(2)	73(4)
MWA	185	60572.540824(18)	1.6(3)	16(2)	64(4)
MWA	185	60572.589281(31)	1.6(4)	21(4)	82(8)
ATCA	2100	60587.270973(26)	0.003(1)	12(2)	0.10(2)
ATCA	2100	60587.319527(28)	0.003(1)	10(3)	0.09(2)
MWA	200	60592.456765(27)	0.7(2)	19(3)	34(3)
MWA	200	60592.505159(33)	0.7(2)	19(4)	35(4)
MWA	200	60593.474369(26)	0.8(2)	15(3)	29(3)
MWA	200	60593.522901(46)	0.6(2)	19(5)	27(4)
MWA	200	60594.443484(21)	0.9(2)	18(2)	43(3)
MWA	200	60594.491990(33)	0.6(3)	12(4)	19(2)
MWA	200	60595.461118(29)	0.7(2)	19(3)	33(3)
MWA	200	60595.509617(25)	0.8(2)	13(3)	27(2)
MWA	200	60596.430283(20)	1.0(2)	16(2)	39(3)
MWA	200	60596.478721(23)	0.9(2)	17(3)	39(3)
MWA	200	60597.447846(41)	0.5(2)	16(5)	22(3)
MWA	200	60597.496319(30)	0.8(2)	19(3)	38(4)
MWA	200	60599.434635(17)	1.2(2)	13(2)	39(2)
MWA	200	60599.483122(24)	1.0(3)	13(3)	32(3)
MWA	200	60600.500655(31)	0.7(2)	16(4)	30(3)
MWA	200	60602.438964(32)	0.7(2)	21(4)	36(4)
MWA	200	60602.487394(27)	0.8(2)	20(3)	39(3)
MeerKAT	813	60602.5835733(40)	0.044(2)	14.9(4)	1.64(4)

This paper has been typeset from a TEX/LATEX file prepared by the author.